Part III

Resultats

Capítol 4

Resultats

plana 77 Purification, crystallization and preliminary X-ray diffraction studies of the bacteriophage ϕ29 connector particle.
A. Guasch, A. Párraga, J. Pous, J.M. Valpuesta, J.L. Carrascosa, and M. Coll.
FEBS Lett, 430:283–287, 1998.

plana 83 Crystallographic analysis reveals the 12-fold symmetry of the bacteriophage ϕ 29 connector particle.
A. Guasch, J. Pous, A. Párraga, J.M. Valpuesta, J.L. Carrascosa, and M. Coll.
J Mol Biol, 281(2):219–225, 1998.

plana 91 Detailed architecture of a DNA translocating machine: The high-resolution structure of the bacteriophage Φ29 connector particle.
J. Pous, A. Guasch, B. Ibarra, F.X. Gomis-Rüth, J.M. Valpuesta, N. Sousa, J.L. Carrascosa and M. Coll.
J Mol Biol 315, 663–676, 2002

Purification, crystallization and preliminary X-ray diffraction studies of the bacteriophage φ29 connector particle

Alicia Guasch[a], Antonio Párraga[a], Joan Pous[a], José M. Valpuesta[b], José L. Carrascosa[b], Miquel Coll[a,*]

1. Introduction

2. Materials and methods and results

2.3. Protein preparation

Thymidylate synthase concentration was 1 mg/ml, and the final concentration of 7 mg/ml, used for crystallization experiments, was reached by two different ways, either by eluting the column with Centricon-10 or by precipitation with ammonium sulfate. With the first method, aggregates depending the sample preparation, significant protein loss was observed due to its binding to the Centricon membrane. The second method consisted in an ammonium sulfate precipitation (0.3 mg/ml) at 4°C, followed by a centrifugation at 4000 × *g*, and dialysis against 0.1 M TrisHCl, 20 mM 2-mercaptoethanol, pH 7.5, 1 mM EDTA. In both cases the same type of crystals were obtained.

The molecular weight of each monomer, determined by mass spectrometry analysis, was 32,800 Da, which coincides with the theoretical molecular weight of the recombinant pET6 protein. However, in some preparations, which resulted in lower quality crystals, the molecular mass showed an increase of 30 Da. To prevent it, 1 mM DTT was added to the protein solution.

The usual protein solution for crystallization contained 7 mg/ml of protein in 0.1 M TrisHCl, 3 mM TrisHCl, pH 7.5. Higher protein concentrations led to the formation of three-dimensional crystals. High salt concentration was crucial to maintain the monomeric in solution.

2.4. Crystallization

Initial conditions for crystallization were obtained by the hanging drop vapor diffusion method upon a broad screening following the conditions of Jancarik and Kim [9] and Carter et al. [10] and included in the Crystal Screening I and II kits (Hampton Research), respectively. The native monomer crystallized in 27% w/v PEG 4000, 20 mM $CaCl_2$, 0.1 M TrisHCl, pH 8.5 at 20°C. The recombinant monomer crystallized in 24–28% isopropyl alcohol, 0.2 M $MgCl_2$, 0.1 M HEPES, pH 7.5 at 20°C.

A modified hollow-wall capillary using parafilm as sealing material to increase the crystal size of the protein-salt complex, keeping constant the drop volume. The optimized protein for crystallization was prepared as follows: 10 μl protein (7 mg/ml in 0.1 M NaCl, 3 mM TrisHCl, pH 7.5, 20 mM 2-ME), 0.5 M $MgCl_2$, 0.1 M HEPES, pH 7.5, and 24 μl pH 7.5, 2 mg/ml. The protein solution was filtered through 0.22 μm Ultrafree-MC at 4°C. Crystallization boxes with plastic hanging rods were used for sealing drop experiments. The methylene depression fill of protein reservoir and of other parafilm of were applied. The bottom of the box was filled with reservoir solution containing initially 24% isopropyl alcohol. Then, it was progressively increased up to 30% isopropylalcohol over 3 days. Following this procedure, clusters crystals (form I) appeared after 4 days and reached a maximum size of approx. 0.2 × 0.2 × 0.1 mm (Fig. 1). In some drops, platelike crystals (forming 0.05 × 0.05 × 0.2 mm crystal form II) appeared simultaneously.

2.5. Data collection and preliminary crystallographic experiments

Both crystals were extremely unstable under the X-rays at 4°C or 20°C and diffracted at a very low resolution (i.e. 10 Å) using a rotating anode source. Under these conditions only a single diffraction image could be taken before complete diffraction decay. However, the flattening of the crystals led to their stabilization and improvement of the diffracting resolution. The flattening procedure was as follows. For crystal form I, each crystal was taken directly from the crystallization drop with an appropriate loop stabilized in specific conditions containing 30% glycerol and flash-frozen directly in the nitrogen stream.

Two native $Hg(CH_3)_2$ derivatives of crystal form II were prepared with different soaking times. A few crystals of $Hg(CH_3)_2$ were introduced in the crystallization drops containing the reservoir crystals. After 2 h a yellowish crystal was taken and flash-frozen directly on the nitrogen stream. The same procedure was repeated within several crystal of intense dark green color after 24 h of soaking.

2.6. Image data collection and processing of crystal form I

Data were collected on a single frozen crystal using a Siemens X-1000 multiwire area detector, using 0.869 Å synchrotron radiation at the DW30 beamline at the LURE, installed on the Positron Accelerator (Orsay, France). Many crystals had to be tested before higher resolution than 3.0 Å could be observed. A 0.5 Å data set was collected at 120 K with a total of 100 frames of 1° oscillation. Data indexing and reduction was performed with XENGEN [11]. Crystal data and diffraction statistics are shown in Tables 1 and 2.

2.7. Crystallographic determination

For the crystal form I, the crystal volume per unit of protein molecular mass (V_m) [12] varies from 4.01 Å³/Da corresponding to 70% solvent to 2.45 Å³/Da for the 30% solvent as the appropriate unit. Because of the size of the parallel and their large central channel it was difficult to estimate a reasonable water content in the crystals. For this reason an experimental determination of density was necessary. The density gradient was measured experimentally using a NaBr gradient according to the method of Hoch and Stellwagen [13]. The protein crystals showed a minimum amount of aqueous channel during centrifugation after successive crystals dehydration steps. The density was determined at the solution point of the slope at 1.30 g/cm³ which implies four monomer particles in the asymmetric unit of the crystal. With 0.3% glutaraldehyde cross-linked crystals the same value was obtained. The V_m value, assuming four monomers in the asymmetric unit, is 3.01 Å³/Da.

2.8. Data collection and processing of crystal form II and derivatives

Native diffraction data for native and $Hg(CH_3)_2$ derivatives of native crystals of form II were collected with a MAR Research imaging plate detector, using 1.309 Å synchrotron radiation at the DW32 beamline of the LURE synchrotron in the Centre Universitaire Paris-Sud, Orsay, France. All data set was collected at 120 K from one crystal with a total of 90° rotation. The distance was set at 180 and 150 mm, respectively. Data indexing and reduction was performed with XENGEN [11]. Crystal data and diffraction statistics are shown in Tables 1 and 2. Two crystallizations of the native protein per unit of protein molecular mass, V_m, is 2.01 Å³/Da, assuming half monomer in the asymmetric unit of the crystal.

3. Discussion

Three-dimensional crystals of the 264 monomer protein can be obtained from alcohol-containing solutions. The strong tendency of the monomers to aggregate in three-dimensional layers has to be prevented by adjusting a precise protein and salt concentration. The removal of minor aggregates or crystal nuclei by filtering the protein solution is also necessary in order to avoid the formation of large two-dimensional crystal layers in the crystallization drops (Fig. 1).

Wedge-shaped crystals of both native and pentahydrated monomers are obtained this way, but the latter grow to larger size and can be stabilized for X-ray data collection. The protein chemical sequence [1] contains 264 residues and 18 residues of the C-terminus. The N-terminal region of 264 monomer is mostly of basic charged residues that could hinder

Table 1
Crystal data

Crystal form	Space group	Cell dimensions (Å)	V_m (Å³/Da)	Molecules/monomers in the asymmetric unit
I	I222	$a=b=c=$ [illegible]	3.01	4/4
II	P4$_1$2$_1$2	$a=b=$ 79.7, $c=$ 134.9	2.01	4/8

Fig. 5. Crystals of the haemagglutinin-HPI monomer obtained with the preadsorbed pH7 protein. Top: Crystals of form I obtained without filtering the protein solution. A background of two-dimensional layers as the ones used for EM studies covers the bottom of the drop. Middle: After filtering the initial pH7 protein solution crystals of form I grew from clear drops and show clear and sharp edges. Bottom: Platelike hexagonal crystals of form II covered the same drops with crystals of form I.

the crystallization process. It is also possible that Fc monomer both N- and C-terminal ends are permeable because the narrow edge of the monomer cylinder [8], the dimensions of the two faces in this region must favor the packing of the particles in the c axis direction, that is, the piling of the monomers along their $[1\,0\,0]$ axis. Then, three-dimensional crystals can be easily

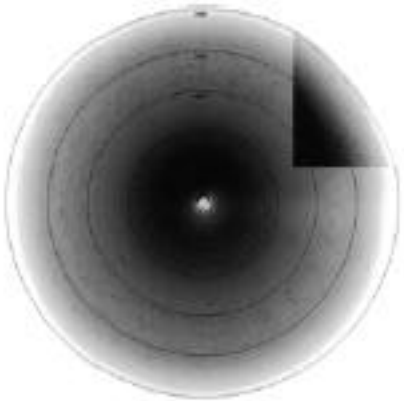

Fig. 1. Diffraction image obtained from a frozen crystal of form II, using synchrotron radiation. The crystal is mounted with the *c* axis approximately parallel to the X-ray beam. Resolution rings are labeled in Å.

over two-dimensional layers, which appear easily in the crystallization drops containing the native protein.

The use of paraffin oil covering the crystallization drops is also critical in order to enlarge the crystals for X-ray diffraction analysis. Without oil, the volume of the drop increases during the crystallization process because a volatile precipitant is used and therefore the protein is diluted during the vapor diffusion experiment. Being the protein concentration already low in the initial setting, the small crystals obtained in drops without oil are unable to grow further. The use of paraffin oil is an efficient alternative crystallization method in chaotropic buffers, which were also tried unsuccessfully in order to prevent the increase in the drop volume. The paraffin oil also extends crystallization by slowing the diffusion into the crystallization drops.

The pH monomer contains two cysteine residues that form a disulfide bridge [L.A. Gilbert, J.M. Valpuesta and J.L. Carrascosa, unpublished results], and we are crystallizing the protein under oxidizing conditions – metal probably at a millimolar concentration – is also important in order to reproduce crystallization. The protein was purified with Ni-metal chromatography, an effective reducing agent that converts millimolar traces to millimolar under reducing conditions [10].

Two crystal forms have been obtained, appearing monoclinic bipyramidal crystallization drops. Although both crystals diffract to high resolution, they display very different diffraction patterns. Crystals of form I diffract anisotropically and usually beyond 3 Å. Even though reflections can be observed up to 2.6 Å resolution, no useful data can be collected in the 6–3.4 Å resolution range. An attempt to do so resulted in low completeness, high R-merge values and unacceptable signal to noise ratio. On the other hand, the crystal form II diffraction intensities can be observed up to 3.2 Å, with good completeness in the last resolution shell and acceptable $\langle I/\sigma(I)\rangle$ values (Table 2). The diffraction pattern (Fig. 2) does not show the strong anisotropy and abnormal intensity drop after 6 Å seen in crystal form I. The crystal form II is a packing arrangement on that described for the two-dimensional sheets of cpn monomers is essential to occur. Electron diffraction patterns obtained from these crystals (like crystals where unit cell parameters of $a=b=180$ Å and 120° symmetry [3], similar to those found in these two-dimensional crystals of form II. An analysis of the internal symmetry of the crystals will be published elsewhere [11]. Crystal of form II will be used for further crystallographic analysis, including the search for new heavy atom derivatives suitable for phasing.

Acknowledgements: This work was supported by the Ministerio de Educación y Ciencia (Grants BIO2004-2211 to J.M.V. and BIO2004-0010 to J.L.C.), by the CIRIT (Pariment exposition 2005-SGR) and the Consejo Superior de Investigaciones Científicas (Grant 200760I270) to J.M.V. Data collection at ESRF-BM16 was supported by the EU Large Installation Project (RII3-CT-2003-506320). We thank P. Bühler for providing the TagHis2 construct and for useful discussions.

References

[1] Valpuesta, J.M. and Carrascosa, J.L. (1994) Q. Rev. Biophys. 27, 107–164.
[2] Clapier, B. and Bowler, B. (2006) in: The Chaperonin (Coles-worker, R.A., Ed.), Vol. 1, pp. 57–91, Nova, New York.
[3] Valpuesta, J.M., Carrascosa, J.L. and Henderson, R. (1994) J. Mol. Biol. 240, 281–287.
[4] Griffiths, D.A.B., Bigot, A., Carrascosa, J.L. and Villa, E.A. (2007) EMBO J. 26, 2374–2383.
[5] Llorca, O., Valpuesta, J.M., Bigot, A., Bruijn, R., Rizo, J., Roise, D., and Carrascosa, J.L. (1992) J. Biol. Chem. 267, 20000–20004.
[6] Llorca, O., Valpuesta, J.M., Silva, F., Rizo, J. and Carrascosa, J.L. (1993) J. Biol. Chem. 268, 20000–20004.

Table 2
Data collection statistics

Crystal form	I	II	Table derivative
Resolution range (Å)	30–3.0	30–3.2	30–3.0
Number of unique reflections	10 991	19 000	5 437
Completeness (%)			
All data	78.7	99.8	98.8
Highest resolution shell (range in Å)	6.93 (3.15–3.0)	99.8 (3.39–3.2)	97.4 (3.15–3.0)
Average redundancy	3.3	3.3	3.7
$I/\sigma(I)$			
All data	3.9	4.3	9.0
Highest resolution shell (range in Å)	0.7 (3.15–3.0)	2.1 (3.39–3.2)	4.2 (3.15–3.0)
R_{merge}			
All data	20.7	17.4	10.7
Highest resolution shell (range in Å)	83.7 (3.15–3.0)	38.9 (3.39–3.2)	19.8 (3.15–3.0)

$^{a}R_{merge}=\sum|I_i-\langle I\rangle|/\sum I_i$, where I_i is the intensity of reflection i and $\langle I\rangle$ is the average I of reflections i and $\sum$ runs over all reflections.

[7] Valpuesta, J.M., [illegible] and Carrascosa, J.L. (1994) EMBO J. 13, [illegible].
[8] [illegible], C., [illegible], J.M., Carrascosa, J.L. and [illegible] (1994) Nucleic Acids Res. [illegible].
[9] Jancarik, J. and Kim, S.H. (1991) J. Appl. Crystallogr. 24, [illegible].
[10] [illegible] (1994) Acta Crystallogr. D [illegible].
[11] [illegible] (1994) Protein Sci. 3, [illegible].
[12] [illegible] (1994) Structure 2, [illegible].
[13] Otwinowski, Z. (1993) DENZO: an Oscillation Data Processing Program for Macromolecular Crystallography, Yale University, New Haven, CT.
[14] Matthews, B.W. (1968) J. Mol. Biol. 33, [illegible].
[15] [illegible], W. and [illegible], T. (1985) Biol. Chem. Hoppe-Seyler [illegible].
[16] [illegible] (1979) [illegible].
[17] Guasch, A., [illegible], Valpuesta, J.M., Carrascosa, J.L. and Coll, M. (1998) J. Mol. Biol. In press.

Article No. mb980 630 J. Mol. Biol. (1998) 280, 223–232

JMB

COMMUNICATION

Crystallographic Analysis Reveals the 12-fold Symmetry of the Bacteriophage φ29 Connector Particle

Alicia Guasch[1], Joan Pous[1], Antonio Parraga[1], José M. Valpuesta[2] José L. Carrascosa[2] and Miquel Coll[1,*]

[1]Departament de Biologia Molecular i Cellular, Centre d'Investigacions Biomèdiques, CSIC Josep Girona, 18-26 08034 Barcelona, Spain

[2]Centro Nacional de Biotecnología, CSIC Universidad Autónoma de Madrid, Cantoblanco 28049 Madrid, Spain

*Corresponding author

The internal symmetry of the connector or portal particle from the double-stranded DNA bacteriophage φ29 has been examined by X-ray crystallography. This large multimeric structure (~310 kDa) is built up by a number of identical subunits of the gp10 protein. It connects the head of the virus with the tail and plays a central role in the protocol assembly and DNA packaging. For the first time a bacteriophage connector has been crystallized and X-ray data have been collected up to a resolution of 3.2 Å. A self-rotation function has been calculated, unambiguously revealing the 12-fold symmetry of the particle and its orientation in the crystal lattice. The orientation has been confirmed by calculating a cross-rotation function using a low resolution model based on electron microscopy reconstructions.

© 1998 Academic Press

Keywords: bacteriophage φ29; connector structure; 12-fold symmetry; X-ray crystallography

φ29 is a complex double-stranded DNA bacteriophage that infects *Bacillus subtilis* cells. The viral particles are formed by a prolate icosahedral capsid, or head, and a tail. Between these two structures there is a connecting region called portal vertex or connector. This head–tail connector plays an important role in the first steps of head assembly and the packaging of DNA. The connector is also involved in the process of DNA transfer into the host cell (for reviews see Cloning & Hendrix, 1988; Valpuesta & Carrascosa, 1994).

The φ29 connector not only interacts with the protocol and the tail, but also with the DNA that is going to be packaged. The DNA binding domain has been located in the N-terminal region of the connector protein gp10, and its removal by treatment with endoglucanase Gln-C from *Staphylococcus aureus* V8 (Gln-C) destroys the generation a connector structure that is unable to bind and package DNA but maintains its quaternary structure (Donate *et al.*, 1993). For the packaging to occur, an RNA of viral origin (prohead RNA or pRNA) is absolutely required (Guo *et al.*, 1987). The RNA binds to the connector and its binding site has been located in the N-terminal region of the protein gp10, not far from the DNA-binding domain (Donate *et al.*, 1993). Finally, an ATPase of viral origin is also required to provide energy to the translocating machinery. This ATPase interacts with the connector although its binding site is not known yet (Valpuesta & Carrascosa, 1994).

The symmetry of the particle

The low resolution three-dimensional structure of the φ29 connector, built up by several copies of the 309 kDa gene 10 product, has been obtained by electron microscopy and image processing of tilted specimens (Carazo *et al.*, 1988). It is composed of two morphological domains: a wider domain of about 145 nm in diameter with protruding lobules and a narrower cylindrical domain of 8 nm in diameter. Running through these two domains, there is a channel of about 4 nm diameter through which the DNA has been hypothesized to enter the viral capsid. The three-dimensional structures of the connector from bacteriophages T3 (Valpuesta *et al.*, 1992) and SPP1 (Tavares *et al.*, 1992) have shown similar general features to that of the φ29 connector. The projection image of several phage connectors (φ29, T3, λ, p22, T4, SPP1) has been obtained from electron microscopy and image processing of tilted specimens. The projection structure of all these connectors, albeit their

*E-mail address of the corresponding author: mmcbbi@cmb.csic.es

0022–2836/98/030223–10 $25.00/0

© 1998 Academic Press

diffuse streaks, like very similar a patent ring surrounding the channel and a set of protruding lobules around the central ring. The difference at the level of position obtained for these connectors (23 to 25 Å) resides in the number of lobules surrounding the central ring and therefore the number of copies upon which the connector is made. In the case of the connectors from phages λ (Lurz *et al.*, 1994), T4 (Steinbacher *et al.*, 1994) and P22 (Bazinet *et al.*, 1988), the results obtained show a clear 12-fold symmetry. In the case of phage connector SPP1 (Orlova *et al.*, 1999), the projection structure reveals a clear 13-fold symmetry. The symmetry of other phage connectors is more controversial and reports postulating 13-fold or 12-fold symmetry have been published for phage connectors ϕ29 (Simon *et al.*, 1986; Ibáñez *et al.*, 1992; Tsuprun *et al.*, 1994; El Khadali *et al.*, 1994; Simon *et al.*, 1993) and T7 (Cerritelli & Studier, 1996). In the case of the ϕ29 connector, a projection obtained at medium resolution (20 Å) using cryoelectron microscopy of unstained two-dimensional crystals (Valpuesta *et al.*, 1994) indicates that the connector has 12 repeat units protruding from a central ring. Recently, the same crystals have been subject to atomic force microscopy studies (Müller *et al.*, 1997) and 12 lobules around the central ring have been found. The discrepancy in the results obtained for the ϕ29 connector have been tried to explain as a result of the non-centrifugal compression of the recombinant connector protein in the bacteria, that could lead to the production of 13-fold or 13-fold symmetry oligomers. Other reports have tried to explain the discrepancy as a result of some of the image processing methods used, which could prevent the identification of the 13-fold symmetric components (Simon *et al.*, 1993). Underlying these discrepancies, there is an important question, as the bacteriophage connector is placed in one of the vertices of the prolate, which has 5-fold symmetry. The mismatch in symmetry between the capsid and the connector has been hypothesized to be an important part of the mechanism of DNA packaging (Hendrix, 1978). To understand the DNA translocating process, it may be important to determine the correct symmetry of the connector.

Three-dimensional crystals diffract up to 3.2 Å

A detailed description of the protein overexpression, connector particle preparation and crystallization will be published elsewhere (Simon *et al.*, 1998). Briefly, the difficulty in obtaining crystals of the ϕ29 connector is that the heavy diffusion arises from the tendency of the connector particles to aggregate in two-dimensional crystal layers at high protein concentration. Only at very precise protein and salt concentrations can the connectors be maintained in solution. Removing aggregation from the protein solution by dilution through 0.22 μm pore filters was also critical in order to obtain high-resolution diffusing three-dimensional crystals. Crystallization was achieved using the vapour diffusion method at 20 °C and sitting drops. Initial crystals of both native and proteolysed connector grown from alcoholic precipitants were too small for X-ray diffraction, likely due to the increase of the drop volume during the crystallization process and the subsequent dilution of the protein concentration in the drop. A modified batch method using paraffin oil (Skow *et al.*, 1994) allowed the increase of crystal size, keeping constant the drop volume. Large crystals could be obtained with the proteolysed connector. Two crystal forms appeared, sometimes in the same drop, depending on the alcohol concentration. Chunky crystals of form I appeared first, after four days, reaching a maximum size of approx. 0.4 mm × 0.3 mm × 0.3 mm. Plate-like crystals of form II have a slower growth habit and grow up to 0.6 mm × 0.6 mm × 0.1 mm. For the structural analysis described here only crystals of this second form were used.

Crystals are normally unstable under the X-ray beam at 20 or 10 °C and diffract to very low resolution (ca. 10 Å) using a rotating anode source. Under these conditions only a single diffraction image could be taken before complete diffraction decay. However, flash-freezing of the crystals led to their stabilization and improvement of the diffracting power. The crystals were taken from the drop with a loop, washed rapidly in a crystallization solution containing 30% (v/v) glycerol and flash-frozen directly under the nitrogen stream. X-ray diffraction data were collected using synchrotron radiation at the EMBL-DESY beamline of the Deutsches Elektronensynchrotron in Hamburg, Germany. Many crystals had to be tested before resolution higher than 6.0 or 7.0 Å could be observed. Crystals of form II diffract to 3.2 Å resolution (Table 1). With these crystals, the intensity of the reflections does not decay sharply beyond 7 Å as in form I (A, diffraction pattern of crystal form II is shown in Figure 2 of Simon *et al.*, 1998). Form II crystals are tetragonal, space group $P4_32_12$ and

Table 1. Data collection statistics

Resolution (Å)	40–3.2
No. of measured reflections	182,149
No. of unique reflections	31,199
Average redundancy	5.8 (5.8)
$\langle I/\sigma(I) \rangle$*	13.7 (3.3)
Completeness (%)	95.8 (95.8)
$I/\sigma(I)$	6.1 (3.4)

Many data statistics of crystal form II. Figures in parentheses are for the outermost 3.31 to 3.2 Å resolution shell. All reflection data were collected from four frozen crystals at 100 K with a MAR Research imaging plate detector using 1.103 Å synchrotron radiation at beamline BW7B at the EMBL outstation at DESY (Hamburg). Data indexing and scaling were performed with DENZO/SCALEPACK (Otwinowski & Minor, 1997).

* $\langle I/\sigma(I) \rangle = \sum_{hkl} \sum_{i} I_i(hkl) / \sum_{hkl} \sum_{i} \sigma_i(hkl)$, where $I_i(hkl)$ are unique reflection values, $\sigma_i(hkl)$ is its measurement estimate and $\langle I(hkl) \rangle$ is the mean intensity of measurements of $I(hkl)$.

(Rossmann & Blow, 1962) as implemented in *GLRF* (Tong & Rossmann, 1997), using polar angles. With *GLRF*, the self-rotation function was calculated using data from 40 Å to 3.5 Å and Patterson vectors up to 40 Å. A very strong peak of value 34σ (second peak = 42, σ = 2.8) appears at $\psi = 90°$, $\phi = 90°$, $\kappa = 30°$ (figure 2b). This peak corresponds to the local 2-fold axis of the particle and is parallel to the crystallographic *c* axis. Perpendicular to it, at section $\kappa = 180°$ and $\phi = 90°$, peaks of the same height (34σ) appear at 15° and 30° on ψ and $\phi = 0°$ (figure 2b). The crystallographic 2-fold axes (2x3) are at $\psi = 0°$, 45°, 90°, $\phi = 0°$ and $\psi = 90°$, $\phi = 90°$ as required for the 422 symmetry. The peaks at 15° and 30° are equivalent to the minimum at section $\kappa = 30°$ (2-fold) and are a consequence of the crystallographic 2-fold axes being exactly perpendicular to the 2-fold local axis of the particle. All these peaks are consistently maintained when varying the resolution range (i.e. using 40 to 6 Å resolution), the integration radius or the self-rotation function grid-sizes (3.2.3). Figure 3 shows a plot of the self-rotation function at $\psi = 90°$, $\phi = 90°$ calculated in either space group *P422* or *P4*. The crystallographic 4-fold axis is seen at $\kappa = 90°$. The local symmetry of the particle is unambiguously 2-fold as indicated by the peaks at $\kappa = 30°$, 60°, 120° and 150°. This rotation function was calculated with data in the resolution range 20 to 6 Å. Using higher resolution data the rotation function results in sharper peaks at the same κ values. A 2-fold local symmetry would show a peak at $\kappa = 72.9°$, which is not the case.

In order to confirm the orientation of the connector particle in the crystals of form II, a cross-rotation function was calculated with AMoRe (Navaza, 1994) using as a starting model the 20 Å

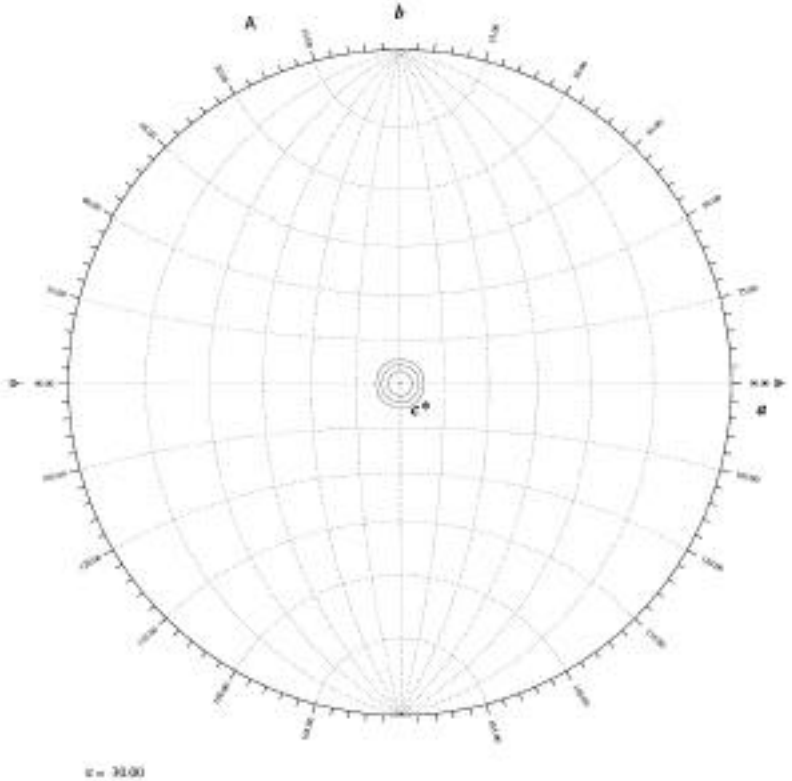

Figure 2 (legend opposite)

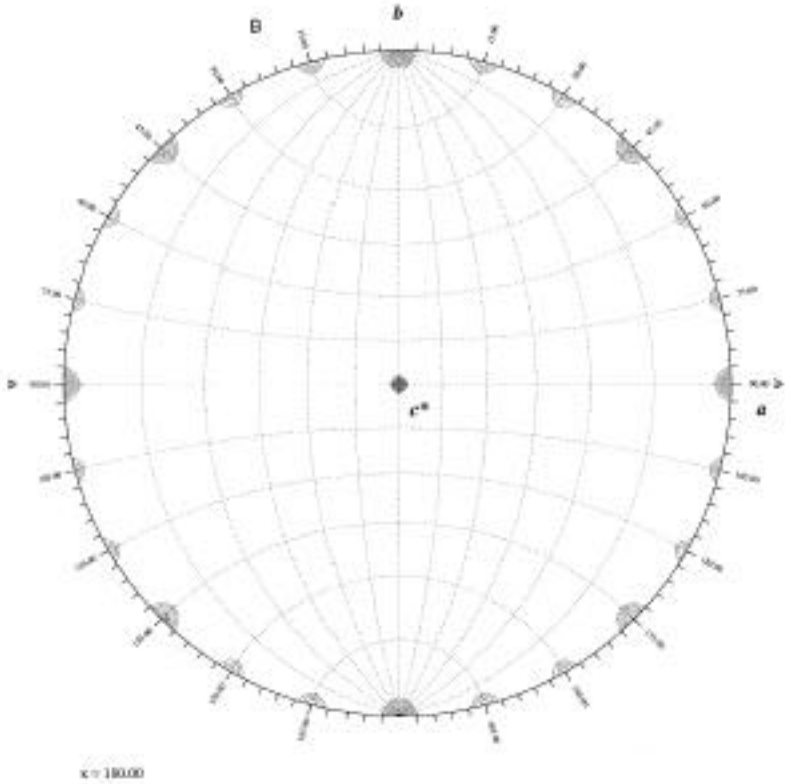

Figure 3. Stereographic projections of the self-rotation function calculated with CCP (Tong & Rossmann, 1997) and viewed along the crystallographic *c* axis. Contour levels are drawn every 0.74 r.m.s. A Sections at $\kappa = 30°$. The peak at $\phi = 90°$, $\phi = 90°$ has a value of 9.65 r.m.s. B Sections at $\kappa = 180°$. The peaks at $\phi = 0°$, $\phi = 0°$ and $\phi = 30°$, $\phi = 0°$ have also a value of 9.65 r.m.s.

diffraction microscopy structure (Carazo *et al.*, 1988). An electron density map was built based on the EM model, oriented with its 12-fold axis parallel to the crystallographic *c* axis and structure factors were calculated with the option MAP of the TAILOR routine in AMoRe. The cross-rotation function between the calculated and the observed amplitudes, computed in the resolution range 30 to 7 Å, gave a set of five similar maxima of value 47 to 49 (correlation coefficient = 0.1 to 7.0) at Eulerian angles $\beta = 60°$, $\gamma = 0°$ and $\alpha = 1.4°$, 14.5°, 28.3°, 61.8° and 70.2°. The highest peak at $\alpha = 61.8°$, $\beta = 60.7°$, $\gamma = 359.0°$ has a value of 7.0 (correlation coefficient = 0.7). Similar results are obtained when using a resolution range from 30 to 10 Å. The same orientation for the particle resulted from the cross-rotation function when using an atomic model, built with atoms randomly filling a 12 Å 3D-model obtained by cryoelectron microscopy (J. M. V. Navarro & J. L. C., unpublished). These results are consistent with the self-rotation function and confirm that the particle is oriented with its 12-fold along the crystallographic *c* axis although the rotation of the particle around its 12-fold is not resolved using this low resolution EM model.

Conclusion

This is the first crystallographic report of a bacteriophage connector or portal particle. The difficulties in obtaining suitable crystals for X-ray diffraction analysis have been overcome by using a protonated gp10 protein which makes a slightly truncated connector cylinder. This probably facili-

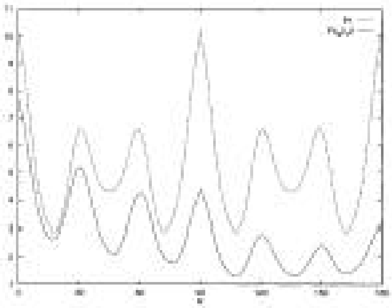

Figure 3. Plot of the self-rotation function at ψ = 90°, calculated in space groups $P4_22_12$ (dotted line) and P1 (continuous line). The function was computed with XPLOR (Brünger, 1992), for the κ interval 1° in 180°, using data from 20 to 5.5 Å and Patterson vectors up to 40 Å. The grid value in κ is 5°.

mize the interlayer interactions, avoiding the formation of bidimensional crystal aggregates. The use of oil in the crystallization drops was also critical in order to enlarge the size of the crystals. High resolution diffraction data, up to 3.2 Å, were obtained from crystal form II, a form that is related to the two-dimensional crystal layers used for previous electron microscopy and atomic force microscopy studies.

The self-rotation and cross-rotation functions allow us to determine the orientation of the particle in the crystal, with its local axis parallel to the crystallographic c axis. The self-rotation function also clarifies a controversial issue showing unambiguously that the internal symmetry of the particle is 12 rather than 13.

Acknowledgements

This work was supported by the Ministerio de Educación y Ciencia (grants [illegible] to M.C. and [illegible] to J.L.C.), by the CSIC (Acciones especiales [illegible]) and the Generalitat de Catalunya (Centre de Referència en Biotecnologia and grant [illegible]). Data collection at EMBL-DESY was supported by the EU Large Installations Project [illegible]. We thank Jorge Navaza for help with AMoRe and Robert Huber for useful discussion.

References

Bazinet, C., Benbasat, J., King, J., Carazo, J. M. & Carrascosa, J. L. (1988). Purification and organization of the gene 1 portal protein required for phage P22 DNA packaging. *Biochemistry*, **27**, 1849–1856.

Bloor, D. M., Chayen, N. E., Lloyd, L. F. & Stainsbie, E. (1994). Control of nucleation of protein crystals. *Protein Sci.* **3**, 1870–1874.

Brünger, A. T. (1992). *X-PLOR, Version 3.1, A System for X-ray Crystallography and NMR*. Yale University Press, New Haven and London.

Carazo, J. M., Donate, L. E., Herranz, L., Secilla, J. P. & Carrascosa, J. L. (1986). Three-dimensional reconstruction of the connector of bacteriophage φ29 at 1.8 nm resolution. *J. Mol. Biol.* **192**, [illegible].

Carrascosa, J. L., Carazo, J. M., Carrascosa, A. L., García, N., Santisteban, A. & Viñuela, E. (1984). General morphology and capsid fine structure of African Swine Fever Virus particles. *Virology*, **132**, 160–172.

Casjens, S. & Hendrix, R. (1988). Control mechanisms in dsDNA bacteriophages. In *The Bacteriophages* (Calendar, R. A., ed.), vol. 1, pp. 15–91, Plenum Publishing Corp., New York.

Cerritelli, M. E. & Studier, F. W. (1996). Purification and characterization of T7 head-tail connectors expressed from the cloned gene. *J. Mol. Biol.* **258**, 299–307.

Donate, L. E., Valpuesta, J. M., Rocher, A., Méndez, E., Rojo, F., Salas, M. & Carrascosa, J. L. (1992). The role of the amino-terminal domain of bacteriophage φ29 connector in DNA binding and packaging. *J. Biol. Chem.* **267**, 10919–10924.

Donate, L. E., Valpuesta, J. M., Mier, C., Rojo, F. & Carrascosa, J. L. (1993). Characterization of a RNA-binding domain in the bacteriophage φ29 connector. *J. Biol. Chem.* **268**, [illegible].

Driedonks, R. A., Engel, A., ten Heggeler, B. & van Driel, R. (1981). Gene 20 product of bacteriophage T4: its purification and structure. *J. Mol. Biol.* **152**, [illegible].

Dube, P., Tavares, P., Lurz, R. & van Heel, M. (1993). The portal protein of bacteriophage SPP1: a DNA pump with 13-fold symmetry. *EMBO J.* **12**, 1303–1309.

Guasch, A., Pous, J., Parraga, A., Valpuesta, J. M., Carrascosa, J. L. & Coll, M. (1998). *FEBS Letters*, in the press.

Guo, P., Erickson, S. & Anderson, D. (1987). A small viral RNA is required for in vitro packaging of bacteriophage φ29 DNA. *Science*, **236**, 690–694.

Hendrix, R. W. (1978). Symmetry mismatch and DNA packaging in large bacteriophages. *Biochemistry*, **75**, 4779–4783.

Huber, R. (1965). Die automatisierte Faltmolekülmethode. *Acta Crystallog.* **19**, 353–356.

Kellenberger, E. (1987). The response of biological macromolecules and supramolecular structures to the physics of specimen cryopreparation. In *Cryotechniques in Biological Electron Microscopy* (Steinbrecht, R. A. & Zierold, Z., eds), pp. 35–63, Springer Verlag, Berlin, Heidelberg.

Kochan, J., Carrascosa, J. L. & Murialdo, H. (1984). Bacteriophage lambda preconnectors. Purification and structure. *J. Mol. Biol.* **174**, 433–447.

Kocsis, E., Cerritelli, M. E., Cheng, N., Trus, B. & Steven, A. C. (1995). Polymorphism of the head to tail connector complex of bacteriophage T3: 12-fold and 13-fold symmetric variants. Proceedings of the XIII International Conference on Virus and Phage Assembly, Sonia, Virginia.

Matthews, B. W. (1968). Solvent content of protein crystals. *J. Mol. Biol.* **33**, 491–497.

Müller, D. J., Engel, A., Carrascosa, J. L. & Vélez, M. (1997). The bacteriophage φ29 head-tail connector imaged at high resolution with the atomic force microscope in buffer solution. EMBO J. 16, 2547–2553.

Navaza, J. (1994). AMoRe: an automated package for molecular replacement. Acta Crystallog. sect. A, 50, 157–163.

Otwinowski, Z. & Minor, W. (1997). Processing of X-ray diffraction data collected in oscillation mode. Methods Enzymol. 276, 307–326.

Rossmann, M. G. & Blow, D. M. (1962). The detection of sub-units within the crystallographic asymmetric unit. Acta Crystallog. 15, 24–31.

Tavares, P., Dröge, A., Lurz, R., Graeber, I., Orlova, E., Dube, P. & van Heel, M. (1995). The SPP1 connection. FEMS Microbiol. Rev. 17, 47–56.

Tong, L. & Rossmann, M. G. (1997). Rotation function calculations with GLRF program. Methods Enzymol. 276, 594–611.

Tsuprun, V., Anderson, D. & Egelman, E. H. (1994). The bacteriophage φ29 head-tail connector shows 13-fold symmetry in both hexagonally packed arrays and as single particles. Biophys. J. 66, 2139–2150.

Valpuesta, J. M. & Carrascosa, J. L. (1994). Structure of viral connectors and their function in bacteriophage assembly and DNA packaging. Quart. Rev. Biophys. 27, 107–155.

Valpuesta, J. M., Fujisawa, H., Marco, S., Carazo, J. M. & Carrascosa, J. L. (1992). Three-dimensional structure of T3 connector purified from overexpressing bacteria. J. Mol. Biol. 224, 103–112.

Valpuesta, J. M., Carrascosa, J. L. & Henderson, R. (1994). Analysis of electron microscope images and electron diffraction patterns of thin crystals of φ29 connectors in ice. J. Mol. Biol. 240, 281–287.

Wrigley, N. G. (1968). The lattice spacing of crystalline catalase as an internal standard in electron microscopy. J. Ultrastruct. Res. 24, 454–464.

Edited by R. Huber

(Received 5 March 1998; received in revised form 11 May 1998; accepted 12 May 1998)